The EMBO Journal (2006) 25, 693–700 | © 2006 European Molecular Biology Organization | All Rights Reserved 0261-4189/06
www.embojournal.org

THE EMBO JOURNAL

Structural basis for myosin V discrimination between distinct cargoes

Natasha Pashkova[1], Yui Jin[1,2], S Ramaswamy[1,*] and Lois S Weisman[1,2,*]

[1]Department of Biochemistry, University of Iowa, Iowa City, IA, USA and [2]Department of Cell and Developmental Biology and Life Sciences Institute, University of Michigan, Ann Arbor, MI, USA

Myosin V molecular motors move cargoes on actin filaments. A myosin V may move multiple cargoes to distinct places at different times. The cargoes attach to the globular tail of myosin V via cargo-specific receptors. Here we report the crystal structure at 2.2 Å of the myosin V globular tail. The overall tertiary structure has not been previously observed. There are several patches of highly conserved regions distributed on the surface of the tail. These are candidate attachment sites for cargo-specific receptors. Indeed, we identified a region of five conserved surface residues that are solely required for vacuole inheritance. Likewise, we identified a region of five conserved surface residues that are required for secretory vesicle movement, but not vacuole movement. These two regions are at opposite ends of the oblong-shaped cargo-binding domain, and moreover are offset by 180°. The fact that the cargo-binding areas are distant from each other and simultaneously exposed on the surface of the globular tail suggests that major targets for the regulation of cargo attachment are organelle-specific myosin V receptors.

The EMBO Journal (2006) **25,** 693–700. doi:10.1038/sj.emboj.7600965; Published online 26 January 2006
Subject Categories: membranes & transport; structural biology
Keywords: cargo-binding domain; membrane transport; myosin V; Myo2p

Introduction

The yeast *Saccharomyces cerevisiae* myosin V motor, Myo2p, attaches to at least six types of cargo, including secretory vesicles, the vacuole/lysosome, late Golgi elements, peroxisomes, mitochondria, and microtubules (Govindan *et al*, 1995; Hill *et al*, 1996; Catlett and Weisman, 1998; Schott *et al*, 1999; Beach *et al*, 2000; Yin *et al*, 2000; Hoepfner *et al*, 2001; Rossanese *et al*, 2001; Boldogh *et al*, 2004; Itoh *et al*, 2004). These cargoes move to distinct locations at different times. Thus, regulation of cargo attachment/detachment and/or regulation of motor activity must specify the appropriate movement of each cargo. Indeed, the discovery of several organelle-specific myosin V receptors demonstrates that organelle-specific myosin V receptors play a major role in the regulation of cargo attachment/detachment (Beach *et al*, 2000; Yin *et al*, 2000; Lapierre *et al*, 2001; Fukuda and Kuroda, 2002; Hume *et al*, 2002; Nagashima *et al*, 2002; Provance *et al*, 2002; Wu *et al*, 2002; Ishikawa *et al*, 2003; Tang *et al*, 2003). Potential roles for the cargo-binding domain of myosin V in cargo attachment have not yet been determined.

The cargo-binding domain of myosin V is composed of subdomains I and II. These domains, residues 1131–1345 (subdomain I) and residues 1346–1574 (subdomain II), were defined by mild proteolysis of the Myo2p globular tail (residues 1087–1574). Notably, all the residues required for Myo2p attachment to the yeast vacuole reside within subdomain I, whereas many of those predicted to be required for Myo2p attachment to secretory vesicles reside within subdomain II (Catlett and Weisman, 1998; Schott *et al*, 1999; Catlett *et al*, 2000; Pashkova *et al*, 2005). Interestingly, each subdomain alone does not have biological activity; however, coexpression of the two subdomains as separate polypeptides *in vivo* results in a functional complex; simultaneous expression of the subdomains has a dominant negative effect and inhibits functions that require Myo2p (Pashkova *et al*, 2005). In addition, subdomains I and II tightly associate with each other. Size-exclusion chromatographic simulations of the reversible dissociation of the subdomains predict that the dissociation equilibrium constant is no greater than 1 nM (Pashkova *et al*, 2005).

To investigate the mechanism whereby myosin V binds diverse cargoes, we crystallized the Myo2p cargo-binding region, the globular tail domain. This study presents the globular tail structure and the identification of two distinct subsets of surface residues required for binding two myosin V cargoes, the vacuole and secretory vesicles, respectively.

Results

Crystallization of the Myo2p globular tail

Numerous trials were performed to identify conditions to produce crystals of the globular tail of Myo2p. Although these failed, we successfully obtained highly diffracting crystals from a trial that had incubated at room temperature for several weeks. We reasoned that mild proteolysis might have occurred, and found that when the full-length tail (residues 1087–1574) was cleaved with trypsin (see Materials and methods), crystals could routinely be obtained. The fact that coexpression of subdomains I and II *in vivo* recapitulates biological functions of the full-length globular tail strongly suggests that the structure reported here is very similar to that of the intact tail.

Indeed, *in vitro* studies comparing the full-length tail with tryptic digests of the tail strongly suggest that the conforma-

*Corresponding authors. S Ramaswamy, Department of Biochemistry, The University of Iowa, Iowa City, IA 52242, USA.
Tel.: +1 319 335 7917; Fax: +1 319 384 4770;
E-mail: s-ramaswamy@uiowa.edu or LS Weisman, Life Sciences Institute, University of Michigan, 210 Washtenaw Avenue, Room 6437, Ann Arbor, MI 48109-2216, USA. Tel.: +1 734 647 2539;
Fax: +1 734 615 5493; E-mail: lweisman@umich.edu

Received: 16 September 2005; accepted: 22 December 2005; published online: 26 January 2006

tions of each are the same. Dynamic light scattering of the Myo2p tail (residues 1131–1574), pre-digested and digested, showed that these proteins have a similar hydrodynamic radius (3.6 and 3.7 nm) and spread of the radius for pre-digested and digested protein samples, respectively. Also under the conditions used, polydispersity was 12.4 and 12.8% for pre-digested and digested protein samples, respectively. The difference in polydispersity values is within the error of the instrument. Polydispersity is a good measure of the flexibility in a protein. A protein that is rapidly sampling two or more conformations would have a larger polydispersity. Monodispersity is an indication that there is possibly a single conformer.

In addition to the above, the behavior during gel filtration of the uncleaved and cleaved polypeptides strongly suggests that they have similar conformations. Using the same column, flow rate, and buffer conditions, the cleaved and uncleaved proteins eluted at identical positions (not shown). Thus, under the experimental conditions of both gel filtration and dynamic light scattering, the Myo2p globular tail and tryptic digest fragments have no observable differences in their conformation.

The current structure includes residues 1152–1274, 1279–1336, 1352–1509, and 1520–1570. The very N-terminal and C-terminal residues are missing. In addition, three small regions within the polypeptide that range in size from 5 to 16 residues are missing as well. It is likely that these interior small regions are loops that connect the α-helices, and that they are less ordered than the rest of the structure. Indeed, MALDI-TOF mass spectrometry of the crystallization sample showed that mild proteolysis had produced several polypeptides that differed by a few amino-acid residues (see Supplementary Figure S1). Note that some of the residues missing from the structure are present in the detected polypeptides, and therefore are likely spatially disordered owing to flexibility in the protein. Other residues missing from the structure are missing from the polypeptide as well and were likely digested during the mild proteolysis or subsequent incubation in the crystallization buffer.

Overall structure of the Myo2p globular tail

The globular tail contains 15 amphipathic α-helices connected by short and long loops (Figure 1A). The architecture reveals two five-helical bundles. The first helical bundle includes H2 to the first half of H6, whereas the second bundle is the distal half of H6–H10 (Figure 1B). These helical bundles correspond to subdomains I and II originally defined by mild proteolysis. The longest helix H6 (45 residues) connects the two helical bundles. A very short helix H11 makes a turn and is followed by two short helices H12 and H13 that together with a hairpin loop form a discrete region at the tip of subdomain II. This region is offset 90° from the helical bundle formed by H6–H10. A long C-terminal loop emerges from H13 and extends along both helical bundles. The C-terminal loop ends with a short helix H15. H15 joins with H1 and H2 and forms a discrete three-helical region at the tip of subdomain I. Based on the crystal structure, it is clear that the Myo2p globular tail subdomain I includes this last short helix. Thus, subdomain I has been revised to include residues 1131–1309 and 1528–1574, and subdomain II is composed of residues 1310–1527.

Like the Myo2p globular tail, both spectrin (Kusunoki *et al*, 2004) and vinculin (Izard *et al*, 2004) have two sets of helical bundles that are connected by a common long helix. However, a search of the PDB did not reveal any proteins with the same architecture as the Myo2p globular tail. We

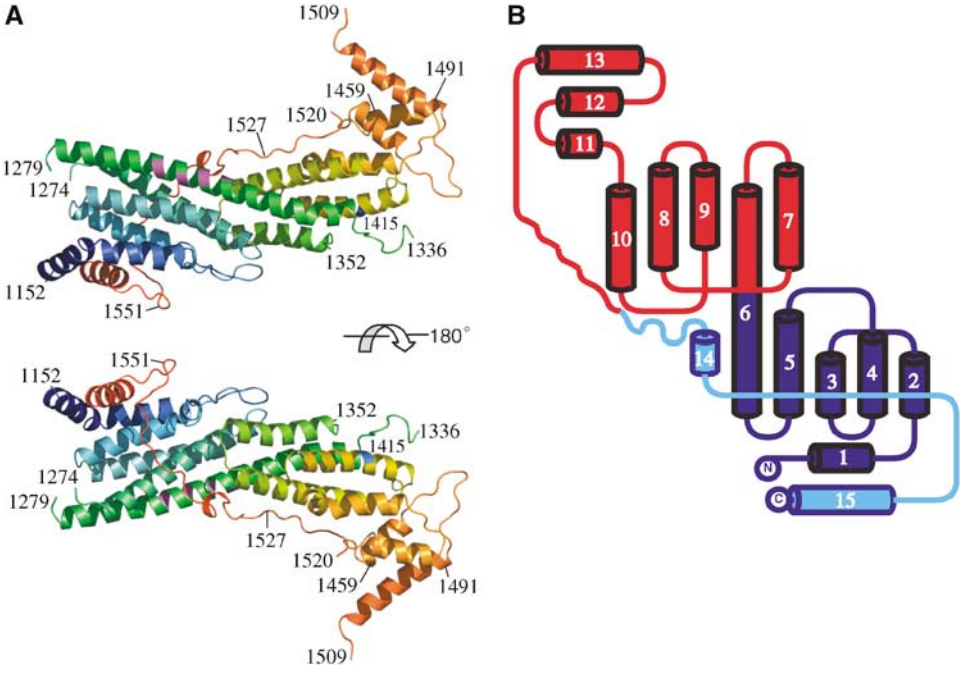

Figure 1 Structural overview of the Myo2p globular tail. (**A**) Ribbon representation of the structure in two orientations (rainbow colors from blue, N-terminus, to red, C-terminus). Vacuole-specific mutations D1297G/N, L1301P, N1304S, and N1307D/N are indicated in magenta. The most amino-terminal residue within the solved structure is 1152. (**B**) Topology diagram. Subdomain I is blue and subdomain II is red. Cyan indicates the region of the C-loop that is part of subdomain I. All structures presented in the figures were drawn using PyMol (DeLano Scientific LLC).

observed a possible internal structural duplication of subdomains I and II. These subdomains show a modest structural similarity to many proteins with α–α superhelices.

Residues from helices H5 and H7 form an extended interface between subdomains I and II. This interface, combined with the extended C-terminal loop that wraps around both subdomains II and I, may explain why the simultaneous expression of each subdomain is required to recapitulate the tested functions of the full-length globular tail (Pashkova *et al*, 2005). In further support that the long C-terminal loop plays an essential role in the structural integrity of Myo2p, deletion of this loop, residues 1519–1574, abolished the binding of the Myo2p tail to its three known binding partners, Vac17p, Kar9p, and Smy1p (Table I; Pashkova *et al*, 2005). In addition, this deletion resulted in a total loss of Myo2p function. Myo2p containing this deletion could not support yeast viability or function in vacuole inheritance (Supplementary Figure S2 and Supplementary Table SI).

Vacuole-binding region

Seven point mutants defective in vacuole inheritance but not secretory vesicle movement have been identified and characterized (Catlett and Weisman, 1998; Catlett *et al*, 2000). These point mutations disrupt binding of the globular tail to Vac17p, a component of the vacuole-specific receptor complex (Ishikawa *et al*, 2003). Notably, six of these point mutations (D1297N/G, L1301P, N1304S/D, and N1307D) cluster to four residues in an 11-amino-acid span. Based on their spacing, we predicted that they lie along a face of an exposed α-helix (Catlett *et al*, 2000). Indeed, these residues are in helix H6, and their side chains point toward the solvent-accessible surface of molecule (Figure 2A).

Based on the structure, it appears that residues from helix H4 may also be part of the vacuole-binding region. Indeed, mutation of a conserved surface residue from H4, Gln1233 to Arg, affected vacuole movement (Figure 2B) but not cell growth. Thus, the vacuole-binding region occupies at least four surface residues from H6 and one residue from H4.

Secretory vesicle-binding region

Analysis of multiple *myo2* temperature-sensitive mutants had predicted that the secretory vesicle-binding region resides in subdomain II of the Myo2 globular tail between residues 1389–1427 and 1439–1491 (Schott *et al*, 1999). This latter region was also suggested by the identification of a secretory vesicle-specific deletion mutant *myo2*-Δ1459–1491. These regions contain many surface residues (Figure 3A), several of which are highly conserved. Point mutations present in the temperature-sensitive mutants that were also highly conserved and exposed to the surface were analyzed further. One residue from the temperature-sensitive mutant *myo2-14* was of particular interest; G1461 resides on the cell surface and is also included in the 1459–1491 deletion. Moreover, it forms a patch with two additional conserved surface residues, D1457 and I1453 (Figure 3A), which are mutated in *myo2-12* and *myo2-18*, respectively. However, we found that the mutants *myo2-G1461D* and *myo2-D1457N* were wild type for growth and for vacuole inheritance (Supplementary Table SI).

In order to map the secretory vesicle-binding region, we analyzed all the surface residues of both subdomains I and II to define areas of high sequence conservation. Myosin V motors from phylogenetically distant species *S. cerevisiae*, *Ustilago maydis*, *Caenorhabditis elegans*, *Drosophila melanogaster*, *Strongylocentrotus purpuratus*, and *Mus musculus* were included in our analysis (Figure 3B). Several large patches of highly conserved surface residues are present in subdomain II. Based on these patches, we constructed and tested *MYO2-R1162E*, *MYO2-D1357K*, *MYO2-E1375V*,

Table I Yeast two-hybrid test of truncation mutants of the Myo2p globular tail with the known Myo2p-binding partners Vac17p, Kar9p, and Smy1p

Myo2p tail	Vac17p	Kar9p	Smy1p
1113–1574	+	+	+
Δ1459–1491	+	–	–
Δ1568–1574	+	+	+
Δ1551–1574	+	–	–
Δ1519–1574	–	–	–

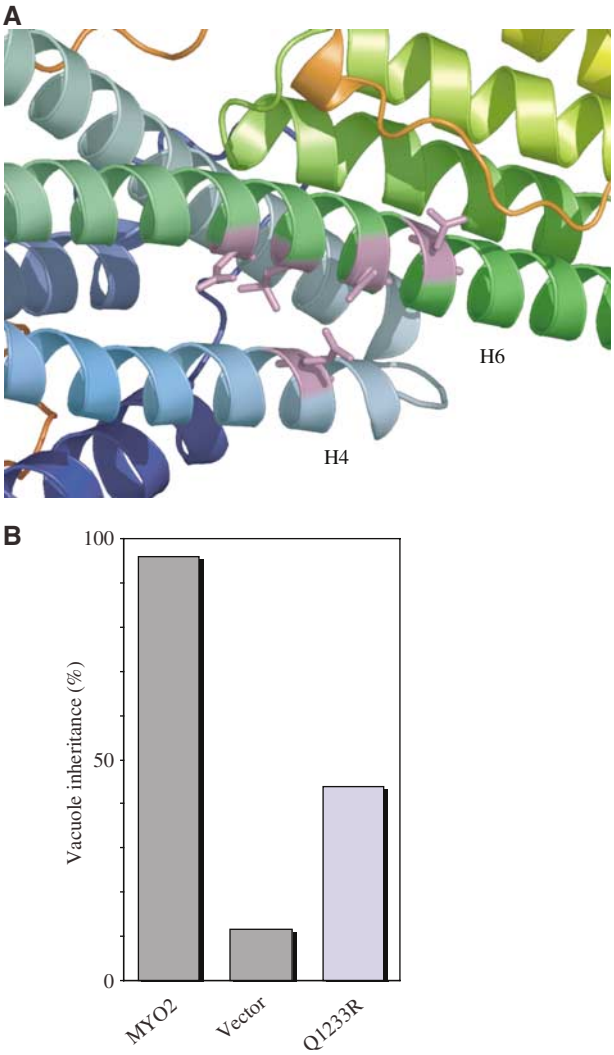

Figure 2 The vacuole-binding region of the globular tail. (**A**) Helices H4 and H6 contain the vacuole-specific residues D1297, L1301, N1304, N1307, and Q1233 (magenta). (**B**) Quantitative analysis of vacuole inheritance of the myo2-Q1233R mutant.

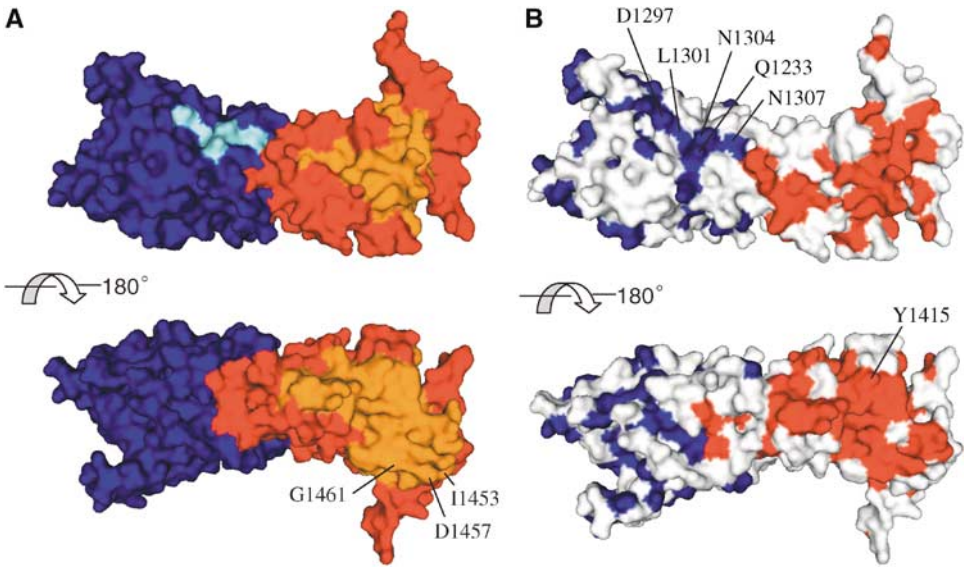

Figure 3 Surface representation of the myosin V globular tail, indicating areas of high sequence conservation. (**A**) Surface area of the Myo2p globular tail conserved region (shown in orange) predicted to bind to secretory vesicles (Schott *et al*, 1999). This region of Myo2p is conserved with chicken myosin Va. The sequence in this region is not conserved with Myo4p, a second *S. cerevisiae* myosin V, which specifically transports mRNA and the peripheral endoplasmic reticulum (Estrada *et al*, 2003). Blue: subdomain I; red: subdomain II; cyan: vacuole-binding region. (**B**) Highly conserved residues (ConSurf scale of '8'or '9') of subdomain I are blue and that of subdomain II in red. Vacuole-specific residues D1297, L1301, N1304, N1307, and Q1233, and the secretory vesicle-specific mutation, Y1415, are indicated.

MYO2-R1402C, *MYO2-K1450I* and *MYO2-Y1415R*. With the exception of *myo2-Y1415R*, each of these mutants was wild type for growth and vacuole inheritance (Supplementary Table SI).

Notably, when either *myo2-Y1415R* or *myo2-Y1415E* were the sole copy of *MYO2, S. cerevisiae* cells were not viable or were temperature sensitive, respectively. These growth defects are most likely due to a defect in the movement of secretory vesicles, the only known essential cargo of Myo2p. However, *myo2-Y1415R* and *MYO2-Y1415E* retained the ability to bind some cargoes. The vacuole inheritance defect of *myo2-2*, a vacuole-specific point mutant, was fully complemented by *myo2-Y1415R* or *myo2-Y1415E* (Supplementary Figure S3). The observation that the *myo2-Y1415R* and *MYO2-Y1415E* alleles support vacuole inheritance indicates that these mutations do not affect the overall structure of the globular tail. These results strongly suggest that Y1415 is part of the secretory vesicle-binding site.

Tests of additional point mutations near Tyr1415 revealed the surface area of the secretory vesicle-binding site. The following mutations in *MYO2*, L1331S, L1411S, K1444A, and Q1447R severely affected yeast growth (Figure 4). Furthermore, another mutation at L1411, *myo2-L1411R*, did not support yeast viability. However, similar to Y1415R, each of the above mutants was fully functional for vacuole movement, and rescued the vacuole inheritance defect of *myo2-2* (not shown). Other point mutations in the region, W1407F, T1418A, E1422A, and K1425A, did not affect yeast growth (Supplementary Table SI), suggesting that the secretory vesicle-binding site does not extend along helix H9.

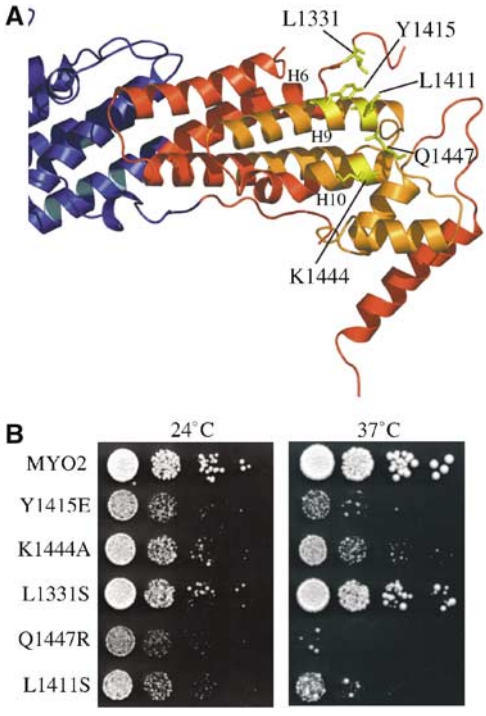

Figure 4 Identification of the secretory vesicle-binding region. (**A**) Ribbon representation of subdomain II. (**B**) Viability assay for secretory vesicle-specific mutants. YEPD plates were incubated at 24 or 37°C. Photographs were taken on day 3.

Discussion

A notable feature of the myosin V tail is the large number of regions of conserved surface residues. Conserved surface residues generally indicate sites of protein–protein interaction. In the case of the myosin V globular tail, at least one of the conserved patches may be required for binding of the myosin V tail to the myosin V motor domain. It was recently found that the motor activity of myosin V is inhibited by interaction of the distal region of the globular tail of

myosin V with the motor domain (Krementsov *et al*, 2004; Li *et al*, 2004; Wang *et al*, 2004). Both analytical ultracentrifugation and rotary shadow electron microscopy revealed two conformations of myosin Va: an 'open' (active) conformation, where the motor domain is available to bind to actin cables and the tail is attached to cargo, and a 'closed' (inactive) conformation where the motor and the cargo-binding domain form a complex with each other. The closed conformation, which occurs in the absence of calcium and cargoes, results in an inhibition of the ATPase activity. These findings strongly suggest that when myosin V is not occupied with cargo, it undergoes a large conformational change that allows the cargo-binding domain to interact with the motor domain and inhibit the ATPase activity of the motor. In further support of this hypothesis, addition of melanophilin to intact myosin Va causes a stimulation of the motor ATPase activity (Li *et al*, 2005).

Note that in the myosin V tail, the conserved patches on subdomain II are significantly larger than the conserved patches on subdomain I (Figure 3B). The reason for this difference is as yet unknown. However, it is tempting to speculate that either of the two large conserved regions on subdomain II may be the site where the motor domain docks. This postulate is based on the assumptions that the interaction between the motor and cargo domain is an ancient, common property of myosin V motors, and also that there might be a large region of contact between the motor- and cargo-binding domains. In an effort to map the region of the globular tail that binds to the motor, we tested whether the yeast two-hybrid assay could be used to monitor an interaction between the Myo2 globular tail and motor domain. Although several regions of the motor and globular tail were tested, none revealed an interaction. It is possible that the neck region is also required for the globular tail to interact with the motor domain (Krementsov *et al*, 2004; Li *et al*, 2004). Alternatively, this interaction may require additional proteins and/or phosphorylation of myosin V tail. Another possibility is that the interaction requires an intact myosin V dimer.

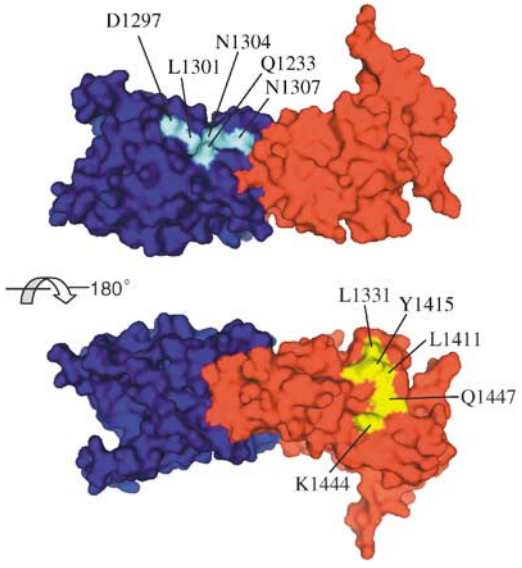

Figure 5 The vacuole- and secretory vesicle-binding sites are structurally separated within the Myo2p globular tail. Surface residues of subdomain I are shown in blue and that of subdomain II in red. Vacuole-binding site is in cyan and secretory vesicle-specific site is in yellow. This present figure and Figure 3 show the same orientation.

Myosin II also undergoes large conformational changes that inhibit its motor ATPase. Hydrodynamic studies of myosin II showed that it exists in two forms, 10S and 6S, which correspond to an open and bent form, respectively (Trybus *et al*, 1982; Ikebe *et al*, 1983). The open form has motor ATPase activity, whereas the closed form is inactive. The mechanism of inhibition requires the dimerization of myosin II and involves the interaction of the converter domain of one head with the actin-binding site of the other head. This conformation blocks the access of each head to actin (Wendt *et al*, 2001; Tama *et al*, 2005). It will be interesting to determine whether the inhibition of myosin V is similarly asymmetric and relies on the fact that it is a dimer.

The microtubule-based conventional kinesin also has a closed, inactive conformation and an open active conformation (Friedman and Vale, 1999; Hackney and Stock, 2000). Kinesin motor activity is inhibited by interaction with the cargo-binding region of the tail. The neck and stalk region of kinesin are also required for this inhibition.

Although the precise mechanism of inhibition of each type of motor is likely to be different, there are at least three properties that each has in common. First, it is of note that each motor is inhibited by the absence of its cargoes. This strongly suggests that it is important that unoccupied motors are inactive. Second, in each case, there are large conformational differences between the active and inactive states. Third, in each case, the motor domain is inhibited through intramolecular interactions, either within the monomer or within a single dimer.

Many of the conserved patches on the surface of the myosin V cargo-binding domain are likely to be regions that bind to specific cargoes. Indeed, the high-resolution structure of the Myo2p cargo-binding domain revealed that the vacuole-specific residues defined by genetic analysis, D1297, L1301, N1304, and N1307 (Catlett *et al*, 2000), lie along a solvent-exposed face of helix 6. These residues comprise most of the vacuole-specific binding region. Based on the structure, we tested adjacent residues on helices 4 and helix 6 and found that Q1233 on helix 4 is also part of the vacuole-binding region.

The high-resolution structure also enabled us to test multiple conserved residues for a specific function in secretory vesicle movement. These studies identified residues L1331, Y1415, L1411, K1444, and Q1447 within one of the conserved patches in subdomain II. The cluster of residues, specific for secretory vesicle movement, occupies a region similar in size to that required for vacuole movement. The exposed residues that make up both vacuole and secretory vesicle-binding sites are highly conserved. The fact that these residues are highly conserved among myosin V motors suggests that these same regions may bind similar organelle-specific receptors in other species. Furthermore, the multiple, as yet undefined additional patches of highly conserved residues on the surface of the globular tail are likely to bind to distinct cargoes.

A major focus in studies of myosin V function is to elucidate the regulatory mechanisms that determine cargo binding. That the secretory vesicle-specific binding region and vacuole-specific binding region are distant from each

other, and are simultaneously exposed on the surface of the globular tail (Figure 5), suggests that the globular tail may not play a major role in the regulation of cargo binding. Rather, the major targets of regulation may be the cargo-specific receptors. Indeed, the vacuole-specific receptor, Vac17p, is synthesized in a cell-cycle-dependent manner (Tang *et al*, 2003). Moreover, turnover of Vac17p results in the detachment of Myo2p and deposits the vacuole in its proper location. In addition, the Myo2p tail interacts much more efficiently with a specific domain of Vac17p (residues 97–170) than with full-length Vac17p (Ishikawa *et al*, 2003), suggesting that a conformational change in Vac17p is required for binding of Vac17p to the globular tail.

To our knowledge, this is the first high-resolution structure of a cargo-binding domain of a molecular motor. The structure of the myosin V globular tail provides a basis for further functional analyses of myosin V.

Materials and methods

Protein purification and crystallization

Recombinant GST-tagged Myo2p globular tail (residues 1087–1574) was cloned and purified as described (Pashkova *et al*, 2005). Briefly, the protein was expressed in *Escherichia coli* BL21(DE3)pLysS cells and purified with Glutathione Sepharose 4B resin (Amersham Biosciences Corp.). After cleavage from GST and dialysis against 20 mM Hepes (pH 6.5), 100 mM NaCl, and 1 mM EDTA buffer, the protein (2 mg/ml) was further treated with 3 μg/ml of trypsin (Sigma-Aldrich) at 0°C for 30 min. The sample was concentrated by spin filtration using an Ultrafree-4 centrifugal filter 30K membrane (Millipore) and purified by gel filtration on a HiLoad 16/60 Superdex 200 prep grade column (Amersham Biosciences Corp.). Selenomethionine-substituted protein was expressed using the methionine pathway inhibition procedure (Doublie *et al*, 1996) and purified as described for the native protein.

Crystals were grown at 4°C by the hanging-drop vapor-diffusion technique using a 1:1 mixture of protein (15–20 mg/ml) and the crystallization solution of 1.7 M NaCl, 8% PEG-6000 for native crystals or 2.2 M NaCl, 8% PEG-6000 for SeMet-substituted crystals. Crystals appeared within 1 week and belonged to space group $P21212_1$ with cell dimensions of 50.7, 72.6, and 167.9 Å (Table II).

Structure determination and refinement

Native data that extended to 2.2 Å resolution were collected at the IMCA-CAT beam line at APS. The structure was determined by the Multiple Anomalous dispersion method. Data from Se-Met crystals were collected at three different wavelengths at the MBC-CAT beam line at ALS in Berkeley. All data were processed using d*trek (Pflugrath, 1999). The positions of selenium were determined and the MAD phases refined using the program SOLVE (Terwilliger and Eisenberg, 1983, 1987; Terwilliger *et al*, 1987; Terwilliger, 1994; Terwilliger and Berendzen, 1997). Density modification and automated model building were carried out with the program RESOLVE (Terwilliger, 2000, 2003). RESOLVE built close to 80% of the side chains that are modeled in the final structure. Further model building was carried out with 'O' (Jones *et al*, 1991), and the structure was refined using the program REFMAC in the CCP4-suite (Murshudov *et al*, 1997). The final *R*-factor and *R*-free are 0.216 and 0.25 respectively using a total of 28 080 unique reflections. A total of 396 residues and 227 water molecules were built. The details of data collection, processing, structure determination, refinement, and quality of the structure are presented in Table II. The coordinates and structure factors have been submitted to the RCSB (PDB ID 2F6H).

Surface conservation analysis

ConSurf algorithms were used to identify evolutionarily conserved surface residues (Glaser *et al*, 2003). Full-length myosin V motors from *S. cerevisiae*, *U. maydis*, *C. elegans*, *D. melanogaster*, *S. purpuratus*, and *M. musculus* were aligned using ClustalW (Thompson *et al*, 1994). Supplementary Figure S4 shows the alignments of the globular tail domain.

Table II Data collection, phasing, and refinement statistics for the Myo2p globular tail

Data collection and phasing	Selenomethionine		Native
	Peak	Inflection point	
No. of crystals	1		1
Total rotation range (deg)	95	95	145
Wavelength (Å)	0.9794	0.9798	1.009
Space group	$P2_12_12_1$		
Cell dimensions (*a*, *b*, *c*) (Å)	50.9, 72.11, 167.85		50.76, 72.57, 167.9
Resolution range (Å)	30.0–2.7 (2.8–2.7)	30.0–2.7 (2.8–2.7)	21.0–2.2 (2.28–2.2)
Mosaicity (deg)	1.77	1.8	0.41
Measured reflections	54 049	54 287	171 687
Unique reflections	16 346	16 330	28 080
Average redundancy	3.3	3.3	5.5 (4.6)
$\langle I\rangle/\langle\sigma(I)\rangle$ [a]	6.7 (2.5)	7.2 (2.8)	8.9 (4.1)
Completeness (%)[a]	90.7 (94.5)	90.5 (94.1)	97.7 (98.5)
R_{merge} (%)[a,b]	12.3 (41.5)	11.6 (39.8)	10.6 (53.2)
Overall *B* factor (Å^2)	49.6	50.6	27.5
Phasing power (acentric)[c]	1.6	1.2	—
Refinement			REFMAC
Resolution limits (Å)			20.0–2.2
Data cutoff, F/σ (*F*)			0
Reflections in working set			26 672
Reflections in test set			1408
R-factor (%)[d]			21.6
R_{free} (%)[e]			24.6
No. of protein atoms			3162
No. of solvent atoms			227
R.m.s. bond lengths (Å)			0.013
R.m.s. bond angles (deg)			1.31
Ramachandran plot (most favored) (%)			93.3

[a]Values in parentheses are for the highest resolution shell.
[b]$R_{merge} = [\sum_{hkl}\sum_i|I_i(hkl)-I(hkl)|/\sum_{hkl}\sum_i I_i(hkl)]$, where $I_i(hkl)$ is the *i*th measurement of reflection *hkl* and $I(hkl)$ its average.
[c]Phasing power = rms ($|F_H|/E$), where *E* is the residual lack of closure.
[d]$R_{factor} = [\sum_{hkl}||F_{obs}|-k|F_{calc}||/\sum_{hkl}|F_{obs}|]$, where F_{obs} and F_{calc} are the observed and calculated structure factor amplitudes, respectively.
[e]R_{free}, same for a test set of reflections not used during refinement.

Site-directed mutagenesis and functional analysis

Yeast *S. cerevisiae* strains used in this study are listed in Supplementary Table SII.

Individual point mutations were generated by the QuikChange Site-Directed mutagenesis method (Stratagene) using pRS413-MYO2. Mutations were verified by sequencing. To assess temperature sensitivity, plasmids with *myo2* mutations or truncations were tested as the sole copy of *MYO2* as described (Catlett *et al*, 2000). Briefly, *S. cerevisiae* cells (LWY2947 strain) with pRS416-MYO2 (URA3) as the sole copy of *MYO2* were transformed with pRS413 (HIS3) containing wild-type or truncated *myo2* (HA tagged). Transformants were streaked onto synthetic media lacking histidine and uracil (SC−His−Ura) to select for the presence of both plasmids, and also streaked onto synthetic media containing 5-fluoroorotic acid (5-FOA) to remove pRS416-MYO2. The resulting strains contain only pRS413-myo2.

To test vacuole inheritance, plasmids with *myo2* mutations or truncations were introduced as a second copy of Myo2p into

LWY5518 strain (Catlett and Weisman, 1998). LWY5518 contains *myo2-2*, which is defective in vacuole movement, but supports yeast viability. Vacuoles were visualized using FM4-64 (Molecular Probes) labeling *in vivo*, as described previously (Catlett *et al*, 2000).

Yeast two-hybrid assay was performed using strain PJ69-4A as described previously (Pashkova *et al*, 2005).

Supplementary data

Supplementary data are available at *The EMBO Journal* Online.

Acknowledgements

This work was supported by grants GM62261 and GM62904 from the National Institutes of Health to LSW and to SR and an American Heart Established Investigator Award (to LSW). We thank Dr L Gakhar and other members of SR laboratory for technical assistance during crystallization and structure analysis. We thank Drs AG Murzin and H Goodson for helpful discussion. We thank Ed Westbrook for kindly collecting excellent MAD data for us in the initial stages of the beam line commissioning. Native data were collected at beam line 17-ID in the facilities of the Industrial Macromolecular Crystallography Association Collaborative Access Team (IMCA-CAT) at the Advanced Photon Source. These facilities are supported by the companies of the Industrial Macromolecular Crystallography Association through a contract with Illinois Institute of Technology (IIT), executed through IIT's Center for Synchrotron Radiation Research and Instrumentation. The Se-Met data were collected at the Molecular Biology Consortium beam line at the Advanced Light Source in Berkeley.

References

Beach DL, Thibodeaux J, Maddox P, Yeh E, Bloom K (2000) The role of the proteins Kar9 and Myo2 in orienting the mitotic spindle of budding yeast. *Curr Biol* **10:** 1497–1506

Boldogh IR, Ramcharan SL, Yang HC, Pon LA (2004) A type V myosin (Myo2p) and a Rab-like G-protein (Ypt11p) are required for retention of newly inherited mitochondria in yeast cells during cell division. *Mol Biol Cell* **15:** 3994–4002

Catlett NL, Duex JE, Tang F, Weisman LS (2000) Two distinct regions in a yeast myosin-V tail domain are required for the movement of different cargoes. *J Cell Biol* **150:** 513–526

Catlett NL, Weisman LS (1998) The terminal tail region of a yeast myosin-V mediates its attachment to vacuole membranes and sites of polarized growth. *Proc Natl Acad Sci USA* **95:** 14799–14804

Doublie S, Kapp U, Aberg A, Brown K, Strub K, Cusak S (1996) Crystallization and preliminary X-ray analysis of the 9 kDa protein of the mouse signal recognition particle and the selenomethionyl-SRP9. *FEBS Lett* **384:** 219–221

Estrada P, Kim J, Coleman J, Walker L, Dunn B, Takizawa P, Novick P, Ferro-Novick S (2003) Myo4p and She3p are required for cortical ER inheritance in *Saccharomyces cerevisiae*. *J Cell Biol* **163:** 1255–1266

Friedman DS, Vale RD (1999) Single-molecule analysis of kinesin motility reveals regulation by the cargo-binding tail domain. *Nat Cell Biol* **1:** 293–297

Fukuda M, Kuroda TS (2002) Slac2-c (synaptotagmin-like protein homologue lacking C2 domains-c), a novel linker protein that interacts with Rab27, myosin Va/VIIa, and actin. *J Biol Chem* **277:** 43096–43103

Glaser F, Pupko T, Paz I, Bell RE, Bechor-Shental D, Martz E, Ben-Tal N (2003) ConSurf: identification of functional regions in proteins by surface-mapping of phylogenetic information. *Bioinformatics* **19:** 163–164

Govindan B, Bowser R, Novick P (1995) The role of Myo2, a yeast class V myosin, in vesicular transport. *J Cell Biol* **128:** 1055–1068

Hackney DD, Stock MF (2000) Kinesin's IAK tail domain inhibits initial microtubule-stimulated ADP release. *Nat Cell Biol* **2:** 257–260

Hill KL, Catlett NL, Weisman LS (1996) Actin and myosin function in directed vacuole movement during cell division in *Saccharomyces cerevisiae*. *J Cell Biol* **135:** 1535–1549

Hoepfner D, van den Berg M, Philippsen P, Tabak HF, Hettema EH (2001) A role for Vps1p, actin, and the Myo2p motor in peroxisome abundance and inheritance in *Saccharomyces cerevisiae*. *J Cell Biol* **155:** 979–990

Hume AN, Collinson LM, Hopkins CR, Strom M, Barral DC, Bossi G, Griffiths GM, Seabra MC (2002) The leaden gene product is required with Rab27a to recruit myosin Va to melanosomes in melanocytes. *Traffic* **3:** 193–202

Ikebe M, Hinkins S, Hartshorne DJ (1983) Correlation of enzymatic properties and conformation of smooth muscle myosin. *Biochemistry* **22:** 4580–4587

Ishikawa K, Catlett NL, Novak JL, Tang F, Nau JJ, Weisman LS (2003) Identification of an organelle-specific myosin V receptor. *J Cell Biol* **160:** 887–897

Itoh T, Toh EA, Matsui Y (2004) Mmr1p is a mitochondrial factor for Myo2p-dependent inheritance of mitochondria in the budding yeast. *EMBO J* **23:** 2520–2530

Izard T, Evans G, Borgon RA, Rush CL, Bricogne G, Bois PR (2004) Vinculin activation by talin through helical bundle conversion. *Nature* **427:** 171–175

Jones TA, Zou JY, Cowan SW, Kjeldgaard M (1991) Improved methods for building protein models in electron density maps and the location of errors in these models. *Acta Crystallogr A* **47** (Part 2)**:** 110–119

Krementsov DN, Krementsova EB, Trybus KM (2004) Myosin V: regulation by calcium, calmodulin, and the tail domain. *J Cell Biol* **164:** 877–886

Kusunoki H, MacDonald RI, Mondragon A (2004) Structural insights into the stability and flexibility of unusual erythroid spectrin repeats. *Structure (Camb)* **12:** 645–656

Lapierre LA, Kumar R, Hales CM, Navarre J, Bhartur SG, Burnette JO, Provance Jr DW, Mercer JA, Bahler M, Goldenring JR (2001) Myosin Vb is associated with plasma membrane recycling systems. *Mol Biol Cell* **12:** 1843–1857

Li XD, Ikebe R, Ikebe M (2005) Activation of myosin Va function by melanophilin, a specific docking partner of myosin Va. *J Biol Chem* **280:** 17815–17822

Li XD, Mabuchi K, Ikebe R, Ikebe M (2004) Ca2 + -induced activation of ATPase activity of myosin Va is accompanied with a large conformational change. *Biochem Biophys Res Commun* **315:** 538–545

Murshudov GN, Vagin AA, Dodson EJ (1997) Refinement of macromolecular structures by the maximum-likelihood method. *Acta Crystallogr D* **53:** 240–255

Nagashima K, Torii S, Yi Z, Igarashi M, Okamoto K, Takeuchi T, Izumi T (2002) Melanophilin directly links Rab27a and myosin Va through its distinct coiled-coil regions. *FEBS Lett* **517:** 233–238

Pashkova N, Catlett NL, Novak JL, Wu G, Lu R, Cohen RE, Weisman LS (2005) Myosin V attachment to cargo requires the tight association of two functional subdomains. *J Cell Biol* **168:** 359–364

Pflugrath JW (1999) The finer things in X-ray diffraction data collection. *Acta Crystallogr D* **55** (Part 10)**:** 1718–1725

Provance DW, James TL, Mercer JA (2002) Melanophilin, the product of the leaden locus, is required for targeting of myosin-Va to melanosomes. *Traffic* **3:** 124–132

Rossanese OW, Reinke CA, Bevis BJ, Hammond AT, Sears IB, O'Connor J, Glick BS (2001) A role for actin, Cdc1p, and Myo2p in the inheritance of late Golgi elements in *Saccharomyces cerevisiae*. *J Cell Biol* **153:** 47–62

Schott D, Ho J, Pruyne D, Bretscher A (1999) The COOH-terminal domain of Myo2p, a yeast myosin V, has a direct role in secretory vesicle targeting. *J Cell Biol* **147:** 791–808

Tama F, Feig M, Liu J, Brooks III CL, Taylor KA (2005) The requirement for mechanical coupling between head and S2 domains in smooth muscle myosin ATPase regulation and its implications for dimeric motor function. *J Mol Biol* **345:** 837–854

Tang F, Kauffman EJ, Novak JL, Nau JJ, Catlett NL, Weisman LS (2003) Regulated degradation of a class V myosin receptor directs movement of the yeast vacuole. *Nature* **422:** 87–92

Terwilliger TC (1994) MAD phasing: bayesian estimates of Fa. *Acta Crystallogr D* **50:** 11–16

Terwilliger TC (2000) Maximum-likelihood density modification. *Acta Crystallogr D* **56** (Part 8)**:** 965–972

Terwilliger TC (2003) Automated side-chain model building and sequence assignment by template matching. *Acta Crystallogr D* **59:** 45–49

Terwilliger TC, Berendzen J (1997) Bayesian correlated MAD phasing. *Acta Crystallogr D* **53:** 571–579

Terwilliger TC, Eisenberg D (1983) Unbiased three-dimensional refinement of heavy-atom parameters by correlation of origin-removed Patterson functions. *Acta Crystallogr A* **39:** 813–817

Terwilliger TC, Eisenberg D (1987) Isomorphous replacement: effects of errors on the phase probability distribution. *Acta Crystallogr A* **43:** 6–13

Terwilliger TC, Kim S-H, Eisenberg D (1987) Generalized method of determining heavy-atom positions using the difference Patterson function. *Acta Crystallogr A* **43:** 1–5

Thompson JD, Higgins DG, Gibson TJ (1994) CLUSTAL W: improving the sensitivity of progressive multiple sequence alignment through sequence weighting, position-specific gap penalties and weight matrix choice. *Nucleic Acids Res* **22:** 4673–4680

Trybus KM, Huiatt TW, Lowey S (1982) A bent monomeric conformation of myosin from smooth muscle. *Proc Natl Acad Sci USA* **79:** 6151–6155

Wang F, Thirumurugan K, Stafford WF, Hammer III JA, Knight PJ, Sellers JR (2004) Regulated conformation of myosin V. *J Biol Chem* **279:** 2333–2336

Wendt T, Taylor D, Trybus KM, Taylor K (2001) Three-dimensional image reconstruction of dephosphorylated smooth muscle heavy meromyosin reveals asymmetry in the interaction between myosin heads and placement of subfragment 2. *Proc Natl Acad Sci USA* **98:** 4361–4366

Wu XS, Rao K, Zhang H, Wang F, Sellers JR, Matesic LE, Copeland NG, Jenkins NA, Hammer III JA (2002) Identification of an organelle receptor for myosin-Va. *Nat Cell Biol* **4:** 271–278

Yin H, Pruyne D, Huffaker TC, Bretscher A (2000) Myosin V orientates the mitotic spindle in yeast. *Nature* **406:** 1013–1015

